

A comprehensive model of gain recovery due to unipolar electron transport after a short optical pulse in quantum cascade lasers

S. E. Jamali Mahabadi, Yue Hu, Muhammad Anisuzzaman Talukder, Thomas F. Carruthers, and Curtis R. Menyuk

Citation: *Journal of Applied Physics* **120**, 154502 (2016); doi: 10.1063/1.4964939

View online: <http://dx.doi.org/10.1063/1.4964939>

View Table of Contents: <http://scitation.aip.org/content/aip/journal/jap/120/15?ver=pdfcov>

Published by the AIP Publishing

Articles you may be interested in

[Loss mechanisms of quantum cascade lasers operating close to optical phonon frequencies](#)

J. Appl. Phys. **109**, 102407 (2011); 10.1063/1.3576153

[Dispersive gain and loss in midinfrared quantum cascade laser](#)

Appl. Phys. Lett. **92**, 081110 (2008); 10.1063/1.2884699

[Impact of doping on the performance of short-wavelength InP-based quantum-cascade lasers](#)

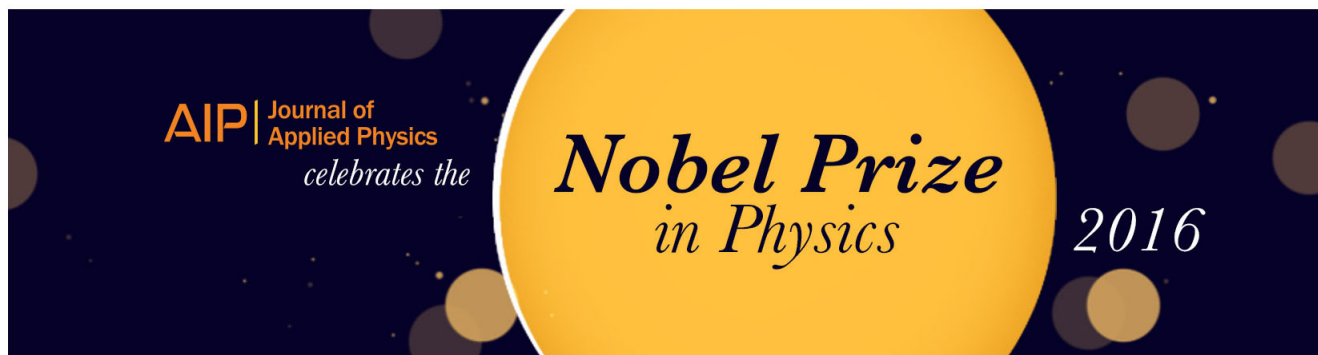
J. Appl. Phys. **103**, 033104 (2008); 10.1063/1.2837871

[Thermal modeling of Ga In As/Al In As quantum cascade lasers](#)

J. Appl. Phys. **100**, 043109 (2006); 10.1063/1.2222074

[Electron-phonon relaxation rates and optical gain in a quantum cascade laser in a magnetic field](#)

J. Appl. Phys. **97**, 103109 (2005); 10.1063/1.1904706



A comprehensive model of gain recovery due to unipolar electron transport after a short optical pulse in quantum cascade lasers

S. E. Jamali Mahabadi,^{1,a)} Yue Hu,¹ Muhammad Anisuzzaman Talukder,^{1,2} Thomas F. Carruthers,¹ and Curtis R. Menyuk¹

¹University of Maryland, Baltimore County 1000 Hilltop Circle, Baltimore, Maryland 21250, USA

²Bangladesh University of Engineering and Technology, Dhaka 1000, Bangladesh

(Received 10 February 2016; accepted 4 October 2016; published online 20 October 2016)

We have developed a comprehensive model of gain recovery due to unipolar electron transport after a short optical pulse in quantum cascade lasers (QCLs) that takes into account all the participating energy levels, including the continuum, in a device. This work takes into account the incoherent scattering of electrons from one energy level to another and quantum coherent tunneling from an injector level to an active region level or vice versa. In contrast to the prior work that only considered transitions to and from a limited number of bound levels, this work includes transitions between all bound levels and between the bound energy levels and the continuum. We simulated an experiment of S. Liu *et al.*, in which 438-pJ femtosecond optical pulses at the device's lasing wavelength were injected into an $\text{In}_{0.653}\text{Ga}_{0.348}\text{As}/\text{In}_{0.310}\text{Al}_{0.690}\text{As}$ QCL structure; we found that approximately 1% of the electrons in the bound energy levels will be excited into the continuum by a pulse and that the probability that these electrons will be scattered back into bound energy levels is negligible, $\sim 10^{-4}$. The gain recovery that is predicted is not consistent with the experiments, indicating that one or more phenomena besides unipolar electron transport in response to a short optical pulse play an important role in the observed gain recovery. *Published by AIP Publishing.*
[\[http://dx.doi.org/10.1063/1.4964939\]](http://dx.doi.org/10.1063/1.4964939)

I. INTRODUCTION

The concept of a superlattice was proposed by Esaki and Tsu in 1970,¹ and in 1994 the first realization of a quantum cascade laser (QCL) based on electron subbands in superlattices was reported by Faist *et al.*² In QCLs, the electron transitions occur between the conduction-band subbands rather than between the conduction and valence bands, so that QCLs are considered to be unipolar devices.³ Electrons in these devices radiatively transfer between the upper and lower subband levels in an active region and subsequently tunnel through an injector region into the upper level of the downstream active region. The tunneling rate, as well as many other performance-related parameters, can be engineered through quantum design.⁴

Light injected into a QCL can change the degree of population inversion and therefore the gain of the device; the device returns to its original equilibrium value with a characteristic gain recovery time.⁵ The gain recovery time is an important parameter for many laser applications, such as creating short pulses by modelocking⁶ and modulating laser light at high speeds for optical communications.⁷

Because carrier transport in QCLs is dominated by ultrafast electron-longitudinal optical (LO) phonon interactions,⁸ it is usually assumed that the gain recovery of QCLs is very fast, on the order of a few picoseconds. The fast gain recovery of QCLs makes it difficult to achieve mode-locking using the conventional techniques,^{9,10} but it allows QCLs to follow changes in the injection current nearly immediately without

relaxation oscillations, which is desirable for a number of applications, including high speed free-space optical communications.⁷ However, Liu *et al.*¹¹ experimentally found that there is a long-term component in the gain recovery of QCLs that at large light intensities is at least 50 ps long. They speculated that this long-term component was due to electron transitions to and from the continuum.

The theoretical study of the gain recovery is important for understanding the physics of QCLs, as well as their behavior in mode-locking or high-speed modulation applications. In this work, we theoretically investigate unipolar electron transport and gain recovery in an $\text{In}_{0.653}\text{Ga}_{0.348}\text{As}/\text{In}_{0.310}\text{Al}_{0.690}\text{As}$ QCL structure that was fabricated by Liu *et al.*⁴ The prior works^{5,12,13} only considered the interaction of the incoming pulse with a limited set of levels—the lasing levels. However, incoming pulses can induce transitions between any two bound levels as well as between the bound levels and the continuum. We have created a model that is comprehensive in the sense that it takes into account *all* these transitions. This model also includes the electron dynamics in the continuum, which must be taken into account in order to properly account for the contribution of the continuum electrons to the gain recovery. The dynamics are complicated because of electron-phonon interactions that lead to rapid thermalization in the electric field that is due to the electrostatic potential. This field is somewhat larger than the field in other quantum well devices such as quantum well infrared photodetectors (QWIPs); however, the processes that govern the continuum electron dynamics are expected to be similar. Electrons that make a transition from bound states to the continuum are originally in the Γ valley, but they will rapidly scatter into the X or L

^{a)}Electronic mail: sjamali1@umbc.edu

valleys due to collisions with phonons, which greatly increases their effective masses.^{14–22} Shortly thereafter, within approximately one period of the QCL, the electrons reach their terminal drift velocity. The wave functions of these electrons are poorly phase-matched to the bound states and only a small fraction of the electrons return to the bound states before they are collected at the cathode.

Our model does not include effects that would lengthen the optical pulse such as facet reflections, temperature changes due to the optical pulse, creation of electron-hole pairs due to high-harmonic generation, and electrical parasitic effects.

We compare our carrier transport and gain recovery results to the experiments that have been carried out on this structure by Liu *et al.*¹¹ We obtain agreement with the short-term gain recovery, which is due to transitions to and from the bound energy levels; its duration is on the order of 2 ps and is consistent with the earlier results of Talukder.⁵ We found that transitions to and from the continuum contribute a longer-term component to the gain recovery with a duration on the order of 10 ps. However, this component contributes on the order of 1% to the gain recovery and is too small to be observable.

Our model does not predict a component to the gain recovery on the order of 50 ps or longer, as is observed in the experiments.¹¹ Since our model includes all known contributions to the gain recovery from unipolar electron transport after a short optical pulse, these results suggest that one or more phenomena other than unipolar electron transport are responsible for the slow gain recovery that is observed. Some possibilities were mentioned earlier.

II. THEORETICAL MODEL

In the pump-probe experiments with QCLs, an ultrashort laser pulse is split into two portions: a stronger beam (pump) is used to excite the sample, generating a nonequilibrium carrier distribution, and a time-delayed weaker beam (probe) is used to monitor the pump-induced changes in the optical parameters, such as reflectivity or transmission, of the sample. Measuring these parameters as a function of the time delay yields information about the relaxation of electronic levels in the sample. Figure 1 schematically illustrates the

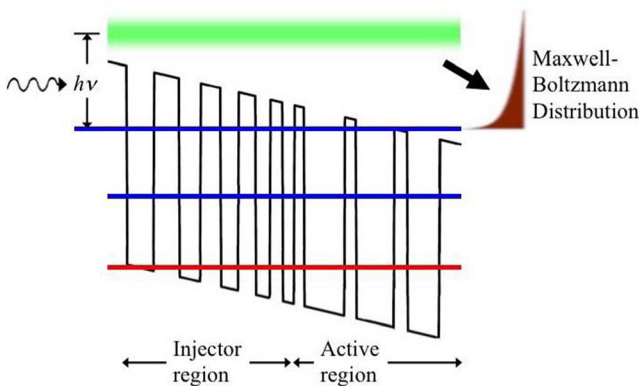


FIG. 1. Illustration of the excitation of electrons to the continuum by an incoming pump pulse and the redistribution of the electron energy to a Maxwell-Boltzmann distribution in the continuum.

excitation of electrons to the continuum by the pump pulse and the redistribution of their energy to a Maxwell-Boltzmann distribution. We will show that this redistribution occurs on a time scale that is similar to the time scale for an electron to move through one period of the device. The thick green line illustrates the finite linewidth of the pump pulse, and the brown inset on the right illustrates the Maxwell-Boltzmann distribution of the electrons in the continuum. The blue curves illustrate wave functions that are primarily in the injector region, and the red curve illustrates a wave function that is primarily in the active region. To find the energy levels, we solve Schrödinger's equation based on the barrier and well heights and widths for the QCL structure. In our model, all the energy levels are excited by an incoming pump pulse with a wavelength equal to the lasing wavelength of the QCL and a duration that is nearly instantaneous. We then calculate the interaction between the incoming pulse and the carrier densities in all the energy levels, and we calculate the subsequent gain recovery. We do not need to include a probe pulse in the model since we directly calculate the recovery of the carrier densities. We write the density matrix equations, which include the incoherent scattering of electrons from one energy level to other energy levels and the coherent tunneling of electrons from an injector region level to an active region level or vice versa. We have extended a previous model^{5,12,13} in which only the interaction of the pump pulse with lasing levels was taken into account. Our new model includes the interaction of the incoming pulse not just with the lasing levels, but also with all the bound state levels. It also includes transitions to and from the continuum, taking into account the dynamics of the continuum electrons.

We used a finite difference method for 1-D discretization of the QCL in the z -direction, which is the growth direction of the QCL, and we used a mid-point method to solve the density matrix equations in time. We formulated and solved the density matrix equations for one active region and two injector regions preceding and following the active region, assuming translational symmetry. The density matrix equations are²³

$$\begin{aligned} \frac{dn_x}{dt} &= \sum_{x \neq x'} \frac{n_{x'}}{s_{x'x}} - \sum_{x \neq x'} \frac{n_x}{s_{xx'}} - i \sum_{x \neq x'} \frac{\Delta_{0,xx'}}{2\hbar} (C_{xx'} - C_{xx'}^*) \\ &\quad + i \sum_{x \neq x'} \frac{\mu_{xx'}}{2\hbar} (\eta_{xx'} \mathcal{E}^* - \eta_{xx'}^* \mathcal{E}) - \sum_x n_x W_x + \sum_x n' W'_x, \\ \frac{dn}{dt} &= \sum_x n_x W_x - \sum_x n' W'_x, \\ \frac{dC_{xx'}}{dt} &= i \frac{\Delta_{0,xx'}}{2\hbar} (n_{x'} - n_x) - \frac{C_{xx'}}{T_{2,xx'}} - i \frac{E_{xx'}}{\hbar} C_{xx'}, \\ \frac{\partial \eta_{xx'}}{\partial t} &= i \frac{\mu_{xx'}}{2\hbar} (n_x - n_{x'}) \mathcal{E} - \left(\frac{1}{T_{2,xx'}} - i \frac{\Delta_{xx'}}{\hbar} \right) \eta_{xx'}, \end{aligned} \quad (1)$$

where n is the carrier density in the bound levels, n' is the carrier density in the continuum, x denotes an energy level, and $C_{xx'}$ denotes the coherence between the energy levels x and x' and has a nonzero value only between an injector level

and an active region level. The quantity $\Delta_{0,xx'}$ is the energy splitting at resonance between levels x and x' that are involved in coherent tunneling and is the minimum energy spacing between the injector and active region levels at the injection and extraction barriers; \mathcal{E} and η are the envelope of the electric field and its polarization, respectively; μ is the dipole moment between the resonant levels; W_x and W'_x are the transition rate of electrons from level x to the continuum and from the continuum to the level x , respectively; $s_{xx'}$ and $T_{2,xx'}$ are the scattering and coherence times between levels x and x' , respectively. We may write

$$\begin{aligned} \frac{1}{s_{xx'}} &= \frac{1}{s_{xx'}^{e-e}} + \frac{1}{s_{xx'}^{e-ph}}, \\ \frac{1}{T_{2,xx'}} &= \frac{1}{T_{2,xx'}^{e-e}} + \frac{1}{T_{2,xx'}^{e-ph}} + \frac{1}{T_{2,xx'}^{e-ir}}, \end{aligned} \quad (2)$$

where $s_{xx'}^{e-e}$ and $s_{xx'}^{e-ph}$ are carrier lifetimes for the transitions due to electron-electron and electron-LO phonon scattering, respectively. The parameters $1/T_{2,xx'}^{e-e}$, $1/T_{2,xx'}^{e-ph}$, and $1/T_{2,xx'}^{e-ir}$ are the rates of the decay of the phase coherence due to electron-electron scattering, electron-LO phonon scattering, and electron-interface roughness scattering, respectively.^{5,13} We also define

$$\begin{aligned} E_{xx'} &= ||E_x - E_{x'}| - \Delta_{0,xx'}|, \\ \Delta_{xx'} &= ||E_x - E_{x'}| - E_{\text{light}}|, \\ E_{\text{light}} &= |E_{\text{ul}} - E_{\text{ll}}|, \end{aligned} \quad (3)$$

where E_x and $E_{x'}$ are the energies of levels x and x' , respectively, while E_{light} , E_{ul} , and E_{ll} are the energy of the incoming light, the energy of upper-lasing level, and the energy of the lower-lasing level, respectively. Hence, $E_x - E_{x'}$ is the energy difference between levels x and x' , $E_{xx'}$ is the detuning of this energy difference from resonance, and $\Delta_{xx'}$ is the detuning of this energy difference from the incident photons.

We computationally excite all the electrons in the subbands of the QCL with an incoming 120-fs, 438-pJ, 4.5- μm optical pulse, which is equal to the device's lasing wavelength. These parameters correspond to the set of experimental parameters at which the pump pulse has the lowest energy.¹¹ We use the Fermi's golden rule²⁴ to calculate electron transition rates W_{if} to and from the continuum, so that

$$\begin{aligned} W_{if} &= \left(\frac{e}{mc}\right)^2 \langle |\mathcal{E}|^2 \rangle \int_{-\infty}^{+\infty} |\mu_{if}|^2 \frac{2\gamma}{|\omega_l - \omega_{if}|^2 + \gamma^2} g(\omega) d\omega, \\ \mu_{if} &= \int_{-\infty}^{+\infty} \psi_f^*(z) \frac{\partial}{\partial z} \psi_i(z) dz, \end{aligned} \quad (4)$$

where W_{if} is the transition rate between the initial level i and the final level f , μ_{if} is the dipole moment between the initial level and final levels, ω_{if} is the angular frequency difference between the initial level and final levels, ω_l is the angular frequency of incoming pulse, γ is the linewidth of the incoming pulse, $g(\omega)$ is density of states, and $\psi_i(z)$ and $\psi_f(z)$ are the wave functions in the initial and final levels, respectively. We solved the Schrödinger's equation for the QCL structure to calculate the bound energy levels and wave functions. To

calculate wave functions in the continuum, we averaged the potential barrier and well height and we approximated them with a slope potential. We validated this approach *a posteriori* using the actual potential and time-independent perturbation theory. With this approximation, Schrödinger's equation in the continuum region becomes

$$\left(-\frac{\hbar^2}{2m^*} \frac{d^2}{dz^2} - eFz\right) \psi_n(z) = E_n \psi_n(z), \quad (5)$$

where e is the electron charge, F is the applied electric field across the QCL, \hbar is Planck's constant, m^* is the electron effective mass, and $\psi_n(z)$ is the wave function corresponding to the eigenenergy E_n . The solution to Eq. (5) can be expressed in terms of Airy functions. Equations (6a) and (6b) show, respectively, the wave functions and eigenenergies

$$\begin{aligned} \psi_n(z) &= CAi \left[\left(\frac{2m^*}{\hbar^2 e^2 F^2} \right)^{1/3} (eFz - E_n) \right], \quad (6a) \\ E_n &= \left(\frac{\hbar^2}{2m^*} \right)^{1/3} \left[\frac{3\pi eF}{2} \left(n - \frac{1}{4} \right) \right]^{2/3}, \quad \text{with } n = 1, 2, \dots, \quad (6b) \end{aligned}$$

where C is a normalization factor and $Ai(x)$ is the Airy function.

For calculating the transition rate between any bound energy level and the continuum, we sum all the transition rates between that bound energy level and a Lorentzian distribution of energy levels in the continuum. When electrons are excited to the continuum, they will be thermalized. In a moderately doped semiconductor sample, the thermal equilibrium energy distribution of the carriers is well-approximated by a Maxwell-Boltzmann distribution.¹⁴ So, to calculate the transition rate from the continuum to the bound levels, we assume that the electrons in the continuum obey a Maxwell-Boltzmann distribution. The electrons in the bound levels are excited to the continuum by the incoming optical pulse. Once the electrons make a transition to the continuum, they rapidly accelerate in a field of 98 kV/cm and their velocities saturate. Due to phonon interactions, the electrons rapidly scatter into the X and L valleys with scattering rates on the order of 10^{13} s^{-1} .²⁵ The maximum velocity of electrons in the device is less than $2 \times 10^7 \text{ cm/s}$ and one period in the device is 35 nm, implying that a continuum electron transits through one period in about $2 \times 10^{-13} \text{ s}$ and is likely to make a transition to the X or L valley in that time. Electrons in the X and L valleys have higher effective masses, and their wave functions are poorly phase-matched to the bound energy levels.

III. SIMULATION RESULTS

Figure 2 shows the conduction band diagram and the moduli-squared wave functions for bound state energy levels in one period of the QCL structure that was studied by Liu *et al.*¹¹ that we are modeling. In this figure, we show one period of the QCL structure that comprises an injector region and an active region. There are four energy levels that are

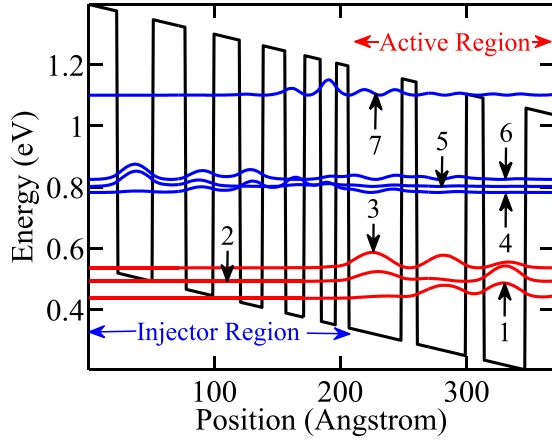


FIG. 2. Moduli-squared wave functions for the bound energy levels for the QCL structure that was fabricated by Liu *et al.*⁴ The thickness of each layer starting from the first active well is as follows (in nanometers): **4.2/1.2/3.9/1.4/3.3/2.3/2.8/2.6/2.2/2.1/1.8/1.8/1.5/1.3/1.2/1.0**. InGaAs quantum wells are in bold and InAlAs quantum barriers are in roman text. The blue curves are wave functions that are primarily in the injector region, and the red curves are wave functions that are primarily in the active region.

primarily in the injector region (shown in blue), and there are three levels that are primarily in the active region (shown in red).

Figure 3(a) shows the transition rates of electrons from the bound levels to the continuum for 43 periods of the QCL structure. Each small circle shows the transition rate for a specific energy level in a specific period. In our calculations, the first period is the period that is closest to the collector,

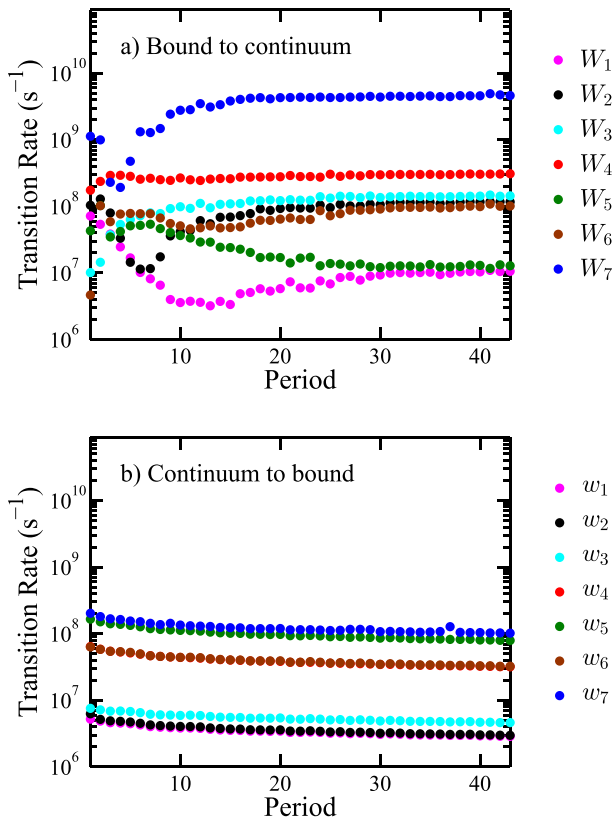


FIG. 3. The transition rates of electrons (a) from energy levels 1–7 (W_1 – W_7) to the continuum summed over 43 periods and (b) to energy levels 1–7 (w_1 – w_7) from the continuum summed over 43 periods.

and we number them successively until we reach the transmitter. The density of states in the continuum above the periods increases as the period number increases, while the cross-section for a transition from a confined state to any particular state in the continuum decreases. We take these two competing effects into account when calculating the transition rate from the confined states in each period into the continuum. We find that for period 20 and higher, these two effects compensate and the transition rate from the same confined state into the continuum becomes the same in each period with a period number greater than 20. Figure 3(a) shows the sum of transition rates from all 43 periods. The variable W_i is the transition rate from energy level i in the bound levels to the continuum. As shown in this figure, level 7 has the highest transition rate to the continuum of all the levels. However, the electron density in level 7 is small compared to the densities in other levels. Transitions from the bound levels to the continuum levels lead to a decrease in the gain. Our simulations show that approximately 1% of the electrons in all the bound levels will be excited to the continuum by an incoming optical pulse whose specifications are given in Table I. All simulation parameters are the same as those used in the pump-probe experiments that we are modeling.¹¹ Figure 3(b) shows the transition rates of electrons from the continuum to the bound levels. The variable w_i is the transition rate to energy level i in the bound levels from the continuum.

We used the first-order time-independent perturbation theory to check the accuracy of approximating the actual potential with a slope potential. We perturbed the slope potential with a correction to take into account the actual barrier potentials that we show in Fig. 2 and calculated the actual wave functions. Figure 4 shows the transition rates of electrons from the bound levels to the continuum for the 43 periods of the QCL structure, when we took the perturbation of the potential into account and used the actual wave functions. As was the case in our calculation of Fig. 3(a), we take into account that the same state in different periods may have a different transition rate. Comparing Figs. 3(a) and 4, we observe that there are quantitative differences between the transition rates, once we take into account the actual barrier potentials. However, when the density in each level is taken into account and we calculate the total transition rate, we still find that only 1% of the electrons make the transition to the continuum. The additional computational complexity in using the actual barrier potential makes little difference in the final result. We note that we use the transition rates corresponding to the actual barrier potentials when calculating the carrier densities, but the difference in the final result when

TABLE I. Simulation parameters from Ref. 11.

Simulation parameter	Parameter value
Pulse width (τ_p)	120 fs
Pulse wavelength	4.5 μm
Pulse energy	438 pJ
Temperature	300 K
Electric field	98 kV/cm

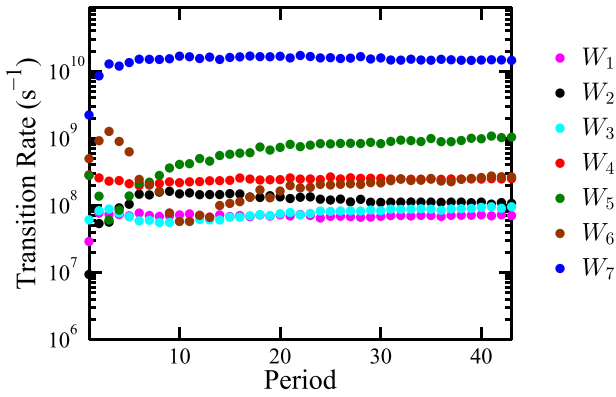


FIG. 4. Transition rates of electrons from energy levels 1–7 (W_1 – W_7) to the continuum summed over 43 periods after perturbing the system.

we use a slope potential is negligible due to the rapid thermalization of the continuum electrons.

Similarly, calculations show that the probability of scattering of the continuum electrons back into the bound levels prior to being collected at the end of the device is negligible ($\sim 10^{-4}$).

Figure 5 shows the time-resolved solutions of Eq. (1), the time evolution of the carrier densities for energy levels 1–3 in the active region and energy levels 4–7 in the injector region. The oscillations in the evolution of carrier densities at the start and during the recovery indicate the presence of significant coherent tunneling in the gain recovery and hence the importance of taking into account the quantum coherence. All the energy levels have initial carrier densities of $4 \times 10^{10} \text{ cm}^{-2}$. After the carrier density in each quantum level reaches a steady state, we initialize the time, setting $t=0$, and we excite all the energy levels with the pump pulse. As can be seen, the carrier density in the upper lasing level (level 4) decreases sharply, while the carrier density in the lower lasing level (level 3) increases sharply. The scattering and coherence times are given in Table II.

Figure 6 shows the carrier density in the continuum as a function of time, which we calculated by solving the drift–diffusion equation²⁶ with an electron drift velocity

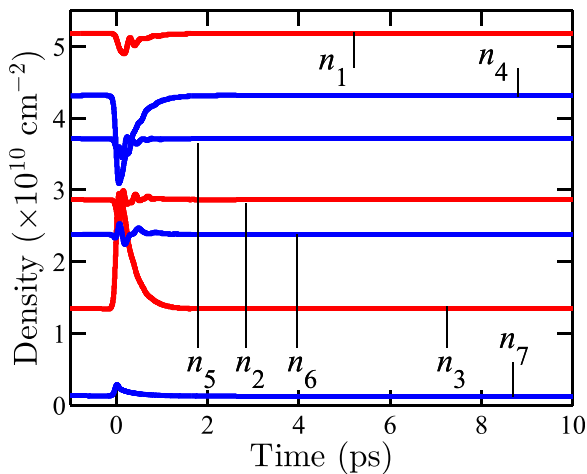


FIG. 5. Carrier densities for energy levels 1–3 in active region and energy levels 4–7 in injector region.

TABLE II. Key parameter values for gain recovery.

Key parameter	Parameter value (ps)
s_{32}	0.60
s_{31}	1.61
s_{21}	0.88
s_{54}	1.13
s_{64}	1.44
s_{74}	6.86
$T_{2,43}$	0.16

$v_n = 1.5 \times 10^7 \text{ cm/s}$ and an electron diffusion coefficient $D_n = 200 \text{ cm}^2/\text{s}$. These are average values for InGaAs and InAlAs,²⁷ which is sufficient for our purposes since the fraction of electrons in the continuum is small.

Figure 7(a) shows the incoming pump pulse and the inversion profile $[n_4(t) - n_3(t)] / (n_{4,\text{eq}} - n_{3,\text{eq}})$, where the subscript “eq” denotes equilibrium and the gain recovery in the pump-probe experiment for the lowest intensity pump pulse in the experiment.¹¹ The inversion profile directly represents the gain recovery dynamics. The gain has a constant value before the pump pulse, but it decreases sharply when the pump pulse interacts with the lasing levels. The recovery of the gain begins as the pump pulse leaves the medium.

In Fig. 7(a), the strong gain depletion near $t=0$ is mainly due to the depletion of electrons in upper lasing subbands by stimulated emission down to the lower lasing level and the excitation of electrons up to a higher subband or continuum region. This process mainly contributes to the gain depletion observed in Fig. 7(a) in agreement with the experimental results.¹¹ Figure 7(b) is an expanded view of Fig. 7(a) near $t=0$ and shows the ultrafast gain recovery, which is due to the depopulation of lower lasing level by LO phonon scattering and electrons filling the upper lasing level by resonantly tunneling from the ground state of the injector region to the active region in the next period through the injector barrier. As can be observed, the simulations reproduce the short-time inversion dip that is observed in the experiments.¹¹ However, there is a significant discrepancy between the experimental and simulation results in Fig. 7(a). The

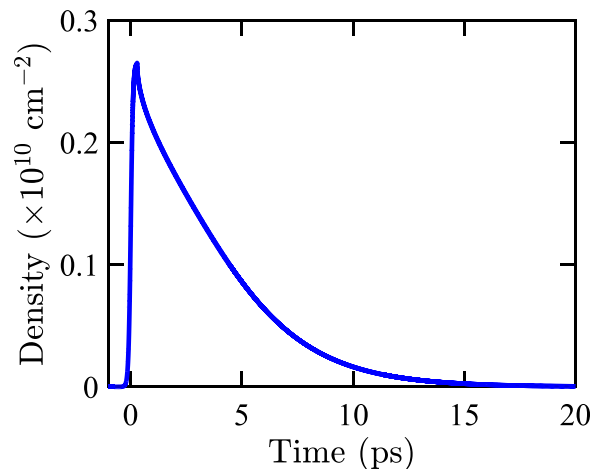


FIG. 6. Carrier density in the continuum as a function of time.

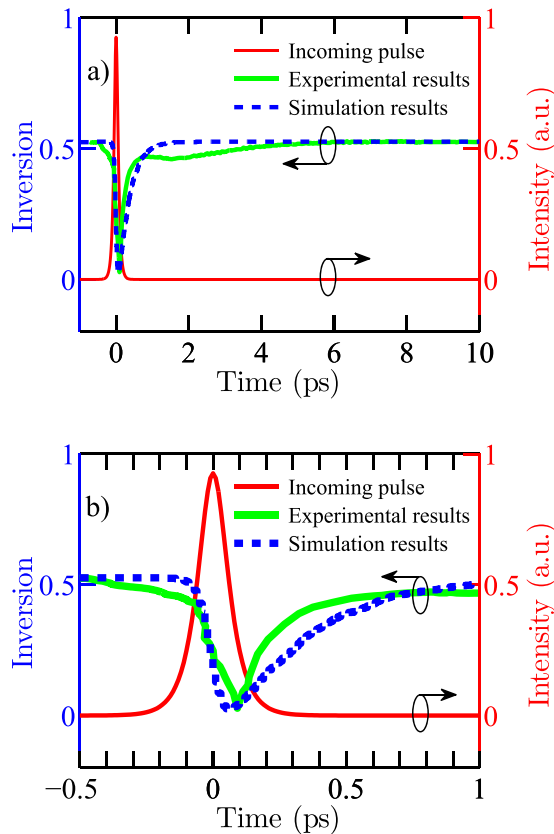


FIG. 7. (a) Inversion (gain) recovery of the QCL with the incoming pump pulse and (b) an expanded view showing the gain recovery in the first picosecond.

experiments exhibit a long-term gain recovery between 1 ps and 6 ps that is not present in the simulations.

There are 43 periods in the QCL structure; each period is 34.6 nm long and the total length of the structure is 1.49 μm . The saturation drift velocity in the continuum region in this structure is on the order of 1.5×10^7 cm/s. The maximum time for electrons to transit through the continuum to the end collector in the 1.49- μm -long device is on the order of 10 ps, and only 1% of electrons make this transition. Therefore, their contribution to the gain recovery is negligible. Liu *et al.*¹¹ also report that at higher optical pump powers, the long-term gain recovery can occur over a time greater than 50 ps and suggest that this long-term recovery might be due to electron transitions into and out of the continuum. Since our model includes all electron transport processes that affect the gain recovery of which we are aware, our results indicate that one or more phenomena besides unipolar electron transport after a short optical pulse are responsible.

IV. CONCLUSIONS

We have developed a comprehensive model of gain recovery in QCLs due to unipolar electron transport after a short optical pulse. This model takes into account all participating energy levels, including the continuum, in a device. We calculated the transition rates of electrons from the bound energy levels to other bound levels and to the continuum after excitation by a short optical pump pulse. We then

calculated the effects of these transitions on gain recovery in the QCL that was studied experimentally by Liu *et al.*¹¹ In agreement with the experimental results, we show that the incoming pulse depletes the lasing levels and reduces the gain. In agreement with these results, we also find that there is a short-term component to the gain recovery that is on the order of 2 ps. This short-term gain recovery is primarily due to electron-electron and electron-phonon scattering to the lasing levels in agreement with a prior theoretical work.⁵ We also show that the gain decrease due to transitions to the continuum is only 1% of the total gain, which is too small to be observable, and the gain recovery from this decrease occurs over 10 ps. In contrast to the experiments, we did not observe a component of the gain recovery on the order of 50 ps or longer. Since our model is comprehensive, in the sense that it includes all electron transitions, this result suggests that one or more phenomena besides unipolar electron transport after a short optical pulse are contributing to the gain recovery.

ACKNOWLEDGMENTS

We gratefully acknowledge the useful discussions with A. M. Johnson and R. A. Kuis and helpful comments by J. B. Khurgin. This work was supported by the MIRTHER NSF Engineering Research Center.

¹L. Esaki and R. Tsu, *IBM J. Res. Dev.* **14**, 61 (1970).

²J. Faist, F. Capasso, D. L. Sivco, C. Sirtori, A. L. Hutchinson, and A. Y. Cho, *Science* **264**, 553 (1994).

³R. Paiella, *Intersubband Transitions in Quantum Structures* (McGraw Hill Professional, New York, 2006).

⁴P. Q. Liu, A. J. Hoffman, M. D. Escarra, K. J. Franz, J. B. Khurgin, Y. Dikmelik, X. Wang, J.-Y. Fan, and C. F. Gmachl, *Nat. Photonics* **4**, 95 (2010).

⁵M. A. Talukder, *J. Appl. Phys.* **109**, 033104 (2011).

⁶H. Haus, *IEEE J. Sel. Top. Quantum Electron.* **6**, 1173 (2000).

⁷F. Capasso, R. Paiella, R. Martini, R. Colombelli, C. Gmachl, T. Myers, M. Taubman, R. Williams, C. Bethea, K. Unterrainer, H. Hwang, D. Sivco, A. Cho, A. Sergent, H. Liu, and E. Whittaker, *IEEE J. Quantum Electron.* **38**, 511 (2002).

⁸J. Faist, F. Capasso, C. Sirtori, D. Sivco, and A. Cho, *Intersubband Transitions in Quantum Wells: Physics and Device Applications II*, edited by H. Liu and F. Capasso (Academic Press, New York, 2000).

⁹A. Gordon, C. Wang, L. Diehl, F. Kärtner, A. Belyanin, D. Bour, S. Corzine, G. Häfner, H. Liu, H. Schneider, T. Maier, M. Troccoli, J. Faist, and F. Capasso, *Phys. Rev. A* **77**, 053804 (2008).

¹⁰M. A. Talukder and C. R. Menyuk, *Phys. Rev. A* **79**, 063841 (2009).

¹¹S. Liu, E. Lalanne, P. Q. Liu, X. Wang, C. F. Gmachl, and A. M. Johnson, *IEEE J. Sel. Top. Quantum Electron.* **18**, 92 (2012).

¹²M. A. Talukder and C. R. Menyuk, *Opt. Commun.* **295**, 115 (2013).

¹³M. A. Talukder and C. R. Menyuk, *New J. Phys.* **13**, 083027 (2011).

¹⁴E. M. Conwell, *High Field Transport in Semiconductors* (Academic Press, New York, 1967).

¹⁵K. W. Böer, *Survey of Semiconductor Physics* (Van Nostrand Reinhold, New York, 1990).

¹⁶A. A. Quaranta, C. Jacoboni, and G. Ottaviani, *Riv. Nuovo Cimento* **1**, 445 (1971).

¹⁷C. Jacoboni, F. Guava, C. Canali, and G. Ottaviani, *Phys. Rev. B* **24**, 1014 (1981).

¹⁸M. Ryzhii, V. Ryzhii, and M. Willander, *J. Appl. Phys.* **84**, 3403 (1998).

¹⁹B. Bouazza, A. Guen-Bouazza, C. Sayah, and N. E. Chabane-Sari, *J. Mod. Phys.* **4**, 121 (2013).

²⁰K. Bhattacharyya, S. M. Goodnick, and J. F. Wager, *J. Appl. Phys.* **73**, 3390 (1993).

²¹E. R. Weber, R. K. Willardson, H. C. Liu, and F. Capasso, *Intersubband Transitions in Quantum Wells: Physics and Device*

- Applications I*, edited by H. C. Liu and F. Capasso (Academic Press, New York, 1999).
- ²²M. Ryzhii and V. Ryzhii, *Appl. Phys. Lett.* **72**, 842 (1998).
- ²³K. Blum, *Density Matrix Theory and Applications* (Springer Science & Business Media, Berlin, 2012).
- ²⁴A. F. J. Levi, *Applied Quantum Mechanics* (Cambridge University Press, New York, 2006).
- ²⁵E. Kobayashi, C. Hamaguchi, T. Matsuoka, and K. Taniguchi, *IEEE Trans. Electron Devices* **36**, 2353 (1989).
- ²⁶R. F. Pierret, *Semiconductor Device Fundamentals* (Pearson Education, India, 1996).
- ²⁷V. Palankovski and R. Quay, *Analysis and Simulation of Heterostructure Devices* (Springer-Verlag, Wien, New York, Austria, 2004).